MANCHESTER 1824
The University of Manchester

The University of Manchester Research

# Aero-optimum hovering kinematics

**DOI:**
10.1088/1748-3190/10/4/044002

**Document Version**
Accepted author manuscript

Link to publication record in Manchester Research Explorer

**Citation for published version (APA):**
Nabawy, M. R. A., & Crowther, W. J. (2015). Aero-optimum hovering kinematics. *Bioinspiration & Biomimetics*, *10*(4), [044002]. https://doi.org/10.1088/1748-3190/10/4/044002

**Published in:**
Bioinspiration & Biomimetics

**Citing this paper**
Please note that where the full-text provided on Manchester Research Explorer is the Author Accepted Manuscript or Proof version this may differ from the final Published version. If citing, it is advised that you check and use the publisher's definitive version.

**General rights**
Copyright and moral rights for the publications made accessible in the Research Explorer are retained by the authors and/or other copyright owners and it is a condition of accessing publications that users recognise and abide by the legal requirements associated with these rights.

**Takedown policy**
If you believe that this document breaches copyright please refer to the University of Manchester's Takedown Procedures [http://man.ac.uk/04Y6Bo] or contact uml.scholarlycommunications@manchester.ac.uk providing relevant details, so we can investigate your claim.


Download date:09. Jun. 2022

# Aero-Optimum Hovering Kinematics

**Mostafa R. A. Nabawy and William J. Crowther**

**School of Mechanical, Aerospace and Civil Engineering, The University of Manchester, Manchester, UK**

## Abstract

Hovering flight for flapping wing vehicles requires rapid and relatively complex reciprocating movement of a wing relative to a stationary surrounding fluid. This note develops a compact analytical aero-kinematic model that can be used for optimisation of flapping wing kinematics against aerodynamic criteria of effectiveness (maximum lift) and efficiency (minimum power for a given amount of lift). It can also be used to make prediction of required flapping frequency for a given geometry and basic aerodynamic parameters. The kinematic treatment is based on a consolidation of an existing formulation that allows explicit derivation of flapping velocity for complex motions whereas the aerodynamic model is based on existing quasi-steady analysis. The combined aero-kinematic model provides novel explicit analytical expressions for both lift and power of a hovering wing in a compact form that enables exploration of a rich kinematic design space. Good agreement is found between model predictions of flapping frequency and observed results for a number of insects and optimal hovering kinematics identified using the model are consistent with results from studies using higher order computational models. For efficient flight, the flapping angle should vary using a triangular profile in time leading to a constant velocity flapping motion, whereas for maximum effectiveness the shape of variation should be sinusoidal. For both cases the wing pitching motion should be rectangular such that pitch change at stroke reversal is as rapid as possible.

**Keywords:** Flapping, kinematics, optimisation, quasi-steady, aerodynamics

## 1. Introduction

Effective hovering flight requires generation of rapid wing motion relative to the stationary surrounding fluid. For helicopter-like vehicles the wing motion is generated relatively simply by continuous rotation of the wing; however, the absence of a viable continuously rotating joint in nature means hoverers have to adopt a reciprocating motion in which the direction and pitch angle of the wing must be reversed at the end of each half-stroke. The fundamental kinematic relations are quite simple: as the wing goes back and forth, the wing should be pitched such that the leading edge is always travelling forward and a positive angle of attack is maintained; however inclusion of non sinusoidal motion primitives makes the problem non trivial. The present work presents a novel formulation of a parameterised analytical aero-kinematic model for hovering flapping flight that can be used in an explicit fashion to evaluate kinematics optimised for different flight performance requirements. The model is also unique in that it can make explicit prediction of the required flapping frequency from relatively basic geometric and weight information. This provides the means for low order design of robotic flying insects or alternatively prediction of flapping frequency of insects from a relatively small number of input parameters. Note that the present study is specific to wing motions of vehicles or animals whose predominant flight mode is hovering and whose wings are thus optimised for hover rather than cruise flight. For animals such as birds and bats who can both cruise and hover with reasonable efficiency, it is common that a different style of hovering is employed in which the half-strokes may be strongly asymmetric.

Identification of optimum flapping kinematics has been the goal of a number of previous studies addressing the aerodynamic efficiency of hovering flapping flight [1-3]. An optimisation problem is typically formulated to identify the wing motion that minimises power expenditure for a given wing while satisfying a weight support (lift) constraint. The aerodynamic models adopted vary from numerical CFD models solving the flow governing equations [3] to the simpler quasi-steady models [1,2]. The main objectives of these studies were typically either to understand insect flying behaviour [1] or to search for flapping motions that are aerodynamically efficient compared to steady fixed wing flight [2,3]. Some studies have varied one or two kinematic parameters at a time to investigate the effect of these wing

kinematic parameters on the aerodynamic performance [4,5], where the aerodynamic performance was assessed based on average lift and average lift to drag ratio values over the flapping cycle. It is reported that lift is increased by increasing flapping frequency, increasing flapping stroke amplitude, and advancing wing pitch rotation [4], and that parameter values for maximum average lift are different to those maximising the average lift to drag ratio [5]. These studies [4,5] did not consider the different possible time shapes of variation for the Euler angles through the flapping cycle [4], or were specific for a linear aerodynamic force coefficient representation [5]. Thus despite allowing insight into the problem, a clear procedure for specification of the kinematics requirements within the engineering design of insect-scale flapping wing vehicles is yet to be defined.

In the following we consider two aspects of aerodynamic performance: optimum kinematics for maximum effectiveness defined in terms of the maximum aerodynamic lift force that can be generated, and optimum kinematics for maximum efficiency defined based on minimising the aerodynamic power expenditure required to generate a given amount of lift. Section 2 defines the motion kinematics and the aerodynamic model upon which the developed aero-kinematic model is based. An interpretation of the developed model is presented in section 3. Section 4 provides results in the form of efficiency and effectiveness maps as a function of motion control parameters and comparison of predicted against actual flapping frequency of a number of different insect species.

## 2. Aero-Kinematic Model

### 2.1 Kinematic motion parameterisation

The kinematics of a rigid wing flapping motion is defined explicitly by three time varying Euler rotations at the shoulder [6] which for insect wing work it is convenient to use the rotation sequence shown in Fig. 1. The flapping stroke angle $\phi(t)$ represents the main forward and backward motion of the wing with respect to the insect frontal plane (plane normal to $z_b$ in Fig. 1). For normal hovering the stroke plane defined by the flapping motion will be horizontal with respect to gravity. Any forward or aft sweep $\varepsilon(t)$

of the wing during flapping will cause the wing to deviate from its original stroke plane, where $\varepsilon(t)$ is referred to as the stroke plane deviation angle. Finally, a rotation $\theta(t)$ is applied about the wing longitudinal axis to alter the geometric angle of attack, $\alpha(t)$, of the wing, where $\theta(t)$ is referred to as the wing pitching angle.

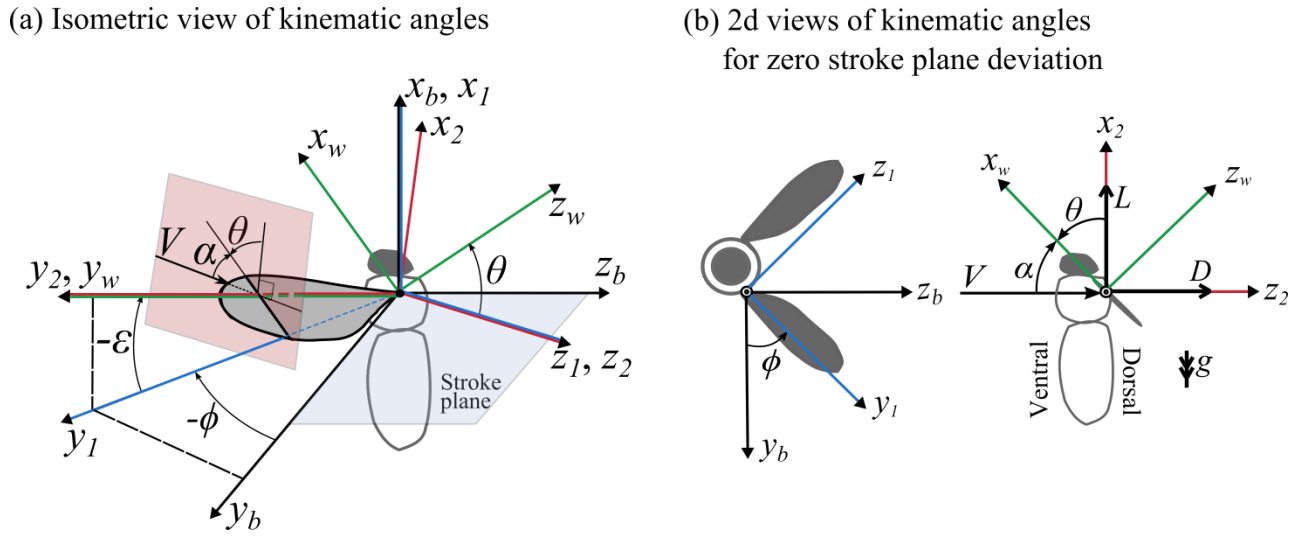


**Figure 1:** (a) The three Euler rotations from the body axes ($x_b$, $y_b$, $z_b$) to the wing axes ($x_w$, $y_w$, $z_w$). (b) For zero stroke plane deviation angle, the axis systems ($x_1$, $y_1$, $z_1$) and ($x_2$, $y_2$, $z_2$) become identical and only two Euler rotations are required from the body to the wing axes. The flapping wing kinematic motion is defined using: the flapping angle, $\phi$, the stroke plane deviation angle, $\varepsilon$ (zero for Fig. 1b), and the wing pitching angle, $\theta$. The angle $\phi$ is a rotation about $x_b$, the angle $\varepsilon$ is a rotation about $z_1$, the angle $\theta$ is a rotation about $y_2$. $L$ denotes lift force and $D$ denotes drag force.

For the present work, we define angle time histories using parameterisations similar to those given by Berman and Wang [1], however we have consolidated the number of parameters to improve the robustness of the motion optimisation process without significant loss of model fidelity. This consolidation is based on the assumption of planar symmetric normal hovering flight in which the wing motion has symmetric half-strokes, where a half-stroke is a complete forward stroke or a complete backward stroke, and the stroke plane deviation angle is zero reducing the required number of motion parameters of Berman and Wang [1] model from 11 to 5. The symmetric normal hovering assumption is justified on the basis that this is a more efficient style of flapping compared to flapping with asymmetric

strokes along an inclined stroke plane (for detailed discussions, see references 7 to 9). The assumption of a planar wing motion is consistent with experimental studies visualising real insect kinematics [6,10-14] where it has been shown that the typical deviation angle amplitudes over the flapping cycle are small and do not make a significant contribution to the generation of primary flight forces.

Following from the above, the time variation of the flapping angle is defined as [1]:

$$\phi(t) = \begin{cases} \phi_{\max} \cos(2\pi f t) & C_\phi = 0 \\ \dfrac{\phi_{\max}}{\sin^{-1} C_\phi} \left( \sin^{-1} \left[ C_\phi \cos(2\pi f t) \right] \right) & 0 < C_\phi \leq 1 \end{cases}. \quad (1)$$

For the aerodynamic model we require the flapping velocity. This is obtained by differentiation of Eqn. 1 to give:

$$\dot{\phi}(t) = \begin{cases} \phi_{\max} \left( -2\pi f \sin(2\pi f t) \right) & C_\phi = 0 \\ \dfrac{\phi_{\max}}{\sin^{-1} C_\phi} \left( -\dfrac{2\pi f C_\phi \sin(2\pi f t)}{\sqrt{1 - C_\phi^2 \cos(2\pi f t)^2}} \right) & 0 < C_\phi \leq 1 \end{cases}. \quad (2)$$

The pitching angle time variation is defined by [1]:

$$\theta(t) = \begin{cases} \theta_{\max} \sin(2\pi f t) & C_\theta = 0 \\ \dfrac{\theta_{\max}}{\tanh C_\theta} \left( \tanh \left[ C_\theta \sin(2\pi f t) \right] \right) & 0 < C_\theta < \infty \end{cases}. \quad (3)$$

The flapping and pitching motion defined in Eqs 1-3 is controlled with five parameters ($\phi_{\max}$, $\theta_{\max}$, $f$, $C_\phi$ and $C_\theta$), where $\phi_{\max}$ is the flapping angle amplitude, $\theta_{\max}$ is the pitching angle amplitude, $f$ is the flapping frequency, and $C_\phi$ and $C_\theta$ are parameters that control the shape of variation of the flapping and pitching cycles respectively. Figure 2 shows range of the kinematic variations that can be simulated with the above motion parameterisation using values of $C_\phi$ and $C_\theta$ set to their bound values. These parameters provide intuitive control parameters for evaluation of feasible engineering designs, and are sufficient to simulate a range of flapping motions relevant to biological studies: Liu and Sun [6] provided

kinematic measurements of hovering droneflies and showed that the flapping angle variation is sinusoidal ($C_\phi \to 0$) whereas the angle of attack could be represented as a constant during the mid half-stroke with a smooth sinusoidal variation at stroke reversal, hence $C_\theta \cong 4$ provides good representation to these results. Similarly, other kinematic measurement studies on hovering honeybees [10] and hovering hoverflies [11] demonstrated a sinusoidal variation for the flapping angle and near constant angle of attack values at mid half-strokes. Elzinga et al. [12] used hovering *Drosophila* kinematics matching a sinusoidal flapping angle variation corresponding to $C_\phi \to 0$ and a near sinusoidal angle of attack variation corresponding to $C_\theta = 1.5$. Kinematic measurements of the hovering hawkmoth [13] also showed a near sinusoidal variation of the flapping angle and an irregular profile for the angle of attack. In a later study [14], this angle of attack variation was approximated with a constant mid-half stroke value and a smooth variation at stroke reversal.

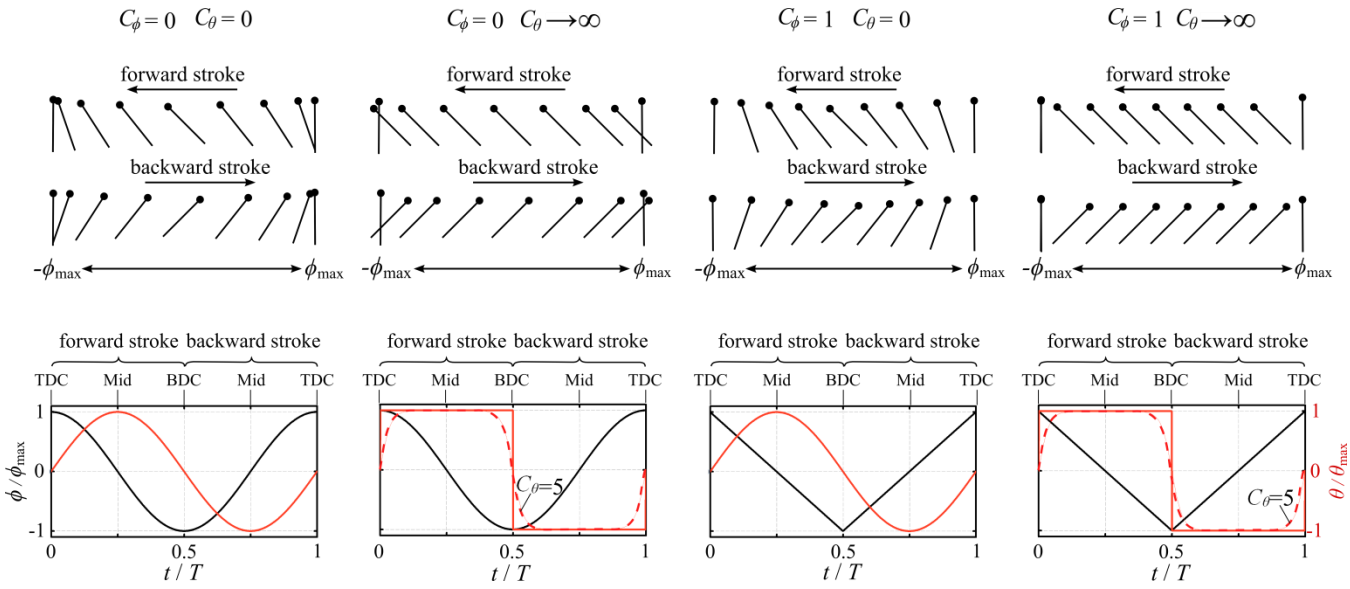


**Figure 2:** Flapping and pitching angle variations during a flapping cycle for different values of $C_\phi$ and $C_\theta$. Stick diagrams of the wing motion are represented for a time interval $0.0625T$. For visualisation purposes, the wing graphic is shown rotated around the mid-chord. The black dots denote the wing leading edge in the graphs. The time variation of the flapping and pitching angles is shown in black and red respectively. TDC denotes Top Dead Centre; BDC denotes Bottom Dead Centre and Mid denotes Mid half-stroke.

## 2.2. Aerodynamic model

### *2.2.1 Generic aerodynamic formulation*

The aerodynamic model adopted in this study is based on a quasi-steady treatment. The lift and drag coefficients, $C_L$ and $C_D$, of the hovering flapping wing are defined within the typical angle of attack, $\alpha$, operation range for insect-like hovering based on the well-established non-linear expressions [1,2,7,15,16]:

$$C_L(\alpha) = C_T \sin(2\alpha), \tag{4}$$

$$C_D(\alpha) = C_L(\alpha)\tan(\alpha) = 2C_T \sin^2(\alpha), \tag{5}$$

where $C_T$ is the translational lift coefficient which depends primarily on the wing shape and Reynolds number [7,15]. Note that Eqs 4 and 5 require two assumptions: Firstly the wing has an un-cambered section with zero twist distribution along the span $\left((C_L)_{\alpha=0} = 0\right)$, which is likely to be valid under normal hovering conditions for most insect wings. Secondly, the skin friction drag on the wing is negligible compared to other drag components including pressure and induced drag $\left((C_D)_{\alpha=0} = 0\right)$, which is consistent with the experimental drag measurements of insect-like flapping wings [16,9,15,1]. For completeness, further justification for assuming a negligible $C_{D0}$ value is included as Appendix A. The current aerodynamic model also ignores the wake capture effect which can be important during start of the flapping half-stroke under some conditions [10]. However, the wing translational phase is the primary contributor to the force generation within the flapping cycle and is alone sufficient to provide weight support [7,15,16].

In the present work, the energetic cost for hovering is given by the mean of positive and negative power output; hence it is assumed that mechanical energy can be stored and released. This is appropriate for most engineering designs where an elastic element can be used to recover the energy [17,18]; though there is some debate on the degree to which this applies in nature. Sun and Du [19] evaluated the inertial contribution for eight hovering insects based on their wing inertial properties and assuming 0% elastic

storage (neglecting negative work) representing the upper limit for inertial contribution. For four insects (fruit fly, cranefly, ladybird and hawkmoth), they found the aerodynamic power much larger than the inertial power, whereas for other four insects (hoverfly, dronefly, honey bee and bumble bee) the calculated inertial power had a significant role and elastic storage can decrease the specific power by approximately 33% [19]. Nevertheless, these results were based on a no elastic storage assumption and several studies show that insects have elastic elements within their bodies that can significantly reduce the inertial power expenditure; for further discussion of this point, the reader is referred to references [20,17]. Thus, the current study will only consider the full elastic storage assumption, which with the employment of symmetric half-strokes leads to a zero net inertial cost. Furthermore, there is a logical path to include inertial contribution in the future for specific cases when inertial and elastic storage characteristics are known. Note that symmetric kinematics leads to zero net force components due to rotational and added mass effects [7,15,21]. Thus, relatively simple analytic formulae to describe the problem can be derived.

Given the symmetry of half-strokes, the hovering lift and power will be based on averaged values during the forward stroke phase. In the forward stroke the time variation of the angle of attack can be written as:

$$\alpha(t) = \frac{\pi}{2} - \theta(t). \tag{6}$$

Using Eqs 2 to 6 within the classical lift and power definitions, it can be shown, after some mathematical manipulation, that the average lift and power can be expressed as:

$$\overline{L} = K_L \int_0^{\frac{1}{2f}} \left(\dot{\phi}(t)\right)^2 \sin(2\alpha(t))dt, \tag{7}$$

$$\overline{P} = K_P \int_0^{\frac{1}{2f}} \left(\dot{\phi}(t)\right)^3 \sin^2(\alpha(t))dt, \tag{8}$$

where

$$K_L = \rho f (R^2 \hat{r}_2^2)(2R\bar{c})(C_T), \tag{9}$$

$$K_P = \rho f (R^3 \hat{r}_3^3)(2R\bar{c})(2C_T), \tag{10}$$

where $\rho$ is the air density, $R$ is the wing length from root to tip, $\bar{c}$ is the mean geometric chord and $\hat{r}_2$, $\hat{r}_3$ are the non-dimensional radii of the second and third moment of wing area respectively.

### *2.2.2 Explicit formulae for average lift and power*

Whilst the lift and power expressions in Eqs 7 and 8 are relatively simple, analytic evaluation of the integrals is not trivial. Nevertheless, with mathematical effort, explicit analytical formulae can be obtained for specific kinematic profiles. These specific profiles include: (1) sinusoidal flapping and pitching angle variations (i.e. $C_\phi = C_\theta = 0$), and (2) rectangular pitching angle variation for any flapping angle variation (i.e. $C_\theta \to \infty$). These profiles allow simplification of the integrand in Eqs 7 and 8, and instead of performing the integration numerically analytical expressions can be obtained for the average lift and power as:

$$\bar{L} = \begin{cases} K_L \left( \frac{16}{3} \pi f \phi_{\max}^2 \theta_{\max} \left( Hypergeom\left[\{2\}, \{\frac{3}{2}, \frac{5}{2}\}, -\theta_{\max}^2\right]\right)\right) & C_\phi = C_\theta = 0 \\ K_L \sin(2\alpha) \left( \left( \frac{C_\phi}{\sin^{-1} C_\phi} \right)^2 \frac{2\pi^2 f \phi_{\max}^2}{1+\sqrt{1-C_\phi^2}} \right) & C_\theta \to \infty \end{cases}, \tag{11}$$

$$\bar{P} = \begin{cases} K_P \left( \frac{8}{3} \pi^2 f^2 \phi_{\max}^3 \left(1 + Hypergeom\left[\{2\}, \{\frac{1}{2}, \frac{5}{2}\}, -\theta_{\max}^2\right]\right)\right) & C_\phi = C_\theta = 0 \\ K_P \sin^2(\alpha) \left(-8\pi^2 f^2 \phi_{\max}^3 \left( \frac{1}{\sin^{-1} C_\phi} \right)^3 \left( C_\phi \sqrt{1-C_\phi^2} - \sin^{-1}\left(C_\phi\right)\right)\right) & C_\theta \to \infty \end{cases}, \tag{12}$$

where *Hypergeom* denotes the hypergeometric function. Note that for the case when $C_\theta \to \infty$, the value of $\alpha$ is constant along the half-stroke and thus is taken out of the integration. Also for this case, the lift and power expressions become singular when $C_\phi$ is zero; however, using a small value of $C_\phi$ (as 0.001)

allows representative simulation of the sinusoidal flapping variation. Using the above equation for lift, the frequency, $f$, can be calculated to satisfy a weight, $W$, requirement as:

$$f = \begin{cases} \sqrt{\dfrac{3W}{\rho(4\phi_{\max} R\hat{r}_2)^2 (2R\bar{c})(C_T)\left(\pi\theta_{\max}\left(Hypergeom\left[\{2\},\{\frac{3}{2},\frac{5}{2}\},-\theta_{\max}^2\right]\right)\right)}} & C_\phi = C_\theta = 0 \\ \sqrt{\dfrac{8W\left(\sin^{-1} C_\phi\right)^2\left(1+\sqrt{1-C_\phi^2}\right)}{\rho\underbrace{(4\phi_{\max} R\hat{r}_2)^2}_{\propto V_{mean}^2}\underbrace{(2R\bar{c})}_{S}\underbrace{(C_T \sin(2\alpha))}_{C_L}(\pi^2 C_\phi^2)}} & C_\theta \to \infty \end{cases} . \quad (13)$$

Equation 13 should prove useful within the design of a flapping wing vehicle as it defines the flapping frequency required to carry a certain total weight for a given wing geometry and kinematic parameters. Substitution of the above frequency relations into Eqn. 12 delivers expressions for the average power for a given weight constraint as:

$$\overline{P} = \sqrt{\frac{3\pi\left(1+Hypergeom\left[\{2\},\{\frac{1}{2},\frac{5}{2}\},-\theta_{\max}^2\right]\right)^2}{32C_T\theta_{\max}^3\left(Hypergeom\left[\{2\},\{\frac{3}{2},\frac{5}{2}\},-\theta_{\max}^2\right]\right)^3}} W^{\frac{3}{2}}\sqrt{\frac{2}{\rho S}}\left(\frac{\hat{r}_3}{\hat{r}_2}\right)^3 \quad C_\phi = C_\theta = 0, \quad (14)$$

$$\overline{P} = \left(\frac{-2\left(C_\phi\sqrt{1-C_\phi^2} - \sin^{-1}\left(C_\phi\right)\right)\left(1+\sqrt{1-C_\phi^2}\right)^{\frac{3}{2}}}{\pi C_\phi^3}\right)\frac{C_D}{C_L^{\frac{3}{2}}} W^{\frac{3}{2}}\sqrt{\frac{2}{\rho S}}\left(\frac{\hat{r}_3}{\hat{r}_2}\right)^3 \quad C_\theta \to \infty. \quad (15)$$

Equation 15 shows that the average power is inversely proportional to the power factor, $PF = C_L^{3/2}/C_D$, which is a measure of the amount of weight that can be supported per unit aerodynamic power [22,2,18]. For a $C_\phi$ value of 0.001 (corresponding to sinusoidal variation of the flapping angle), Eqn. 15 reduces to:

$$\overline{P} = 1.2W^{\frac{3}{2}}\sqrt{\frac{2}{\rho S}}\frac{C_D}{C_L^{\frac{3}{2}}}\left(\frac{\hat{r}_3}{\hat{r}_2}\right)^3. \quad (16)$$

Whilst for a unity $C_\phi$ value corresponding to constant angular velocity variation with respect to time, Eqn. 15 reduces to:

$$\overline{P} = W^{\frac{3}{2}} \sqrt{\frac{2}{\rho S}} \frac{C_D}{C_L^{\frac{3}{2}}} \left( \frac{\hat{r}_3}{\hat{r}_2} \right)^3 . \tag{17}$$

Equations 16 and 17 are consistent with the final results of Taha et al. [18]; and apart from the appearance of the term containing $\hat{r}_2$ and $\hat{r}_3$ due to the linear variation of the sectional velocity along the wing length (i.e. $V(r) = \dot{\phi} r$), Eqn. 17 is the same as the well-know aerodynamic power relation for steady flight of fixed wing vehicles. Whilst the previous does not validate the model in anyway, it does provide circumstantial evidence that the analytical approach is sound.

## 3. Model Interpretation

### 3.1 Selection of flapping profile

Before progressing to evaluation of the complete aerodynamic model as a function of both flapping and pitching control parameters ($C_\phi$ and $C_\theta$), it is instructive to consider the implications of changing flapping kinematics using a simple case in which the pitch change at the end of each half-stroke is instantaneous ($C_\theta \to \infty$) such that the geometric angle of attack is constant during each half-stroke. From inspection of Eqn. 7 it can be seen that with the flapping velocity, $\dot{\phi}$, as the only variable, the lift will be proportional to the *mean square* of the flapping velocity over the flapping cycle. Consider the two flapping profiles given by $C_\phi = 0$ and $C_\phi = 1$ corresponding to a sinusoidal and triangular motion, respectively. For a given flapping frequency and stroke amplitude the sinusoidal profile will have the higher mean square value, hence we would anticipate that solutions for high effectiveness obtained from the complete model will be biased towards sinusoidal flapping profiles. If we now consider efficiency as the goal, measured in terms of power/lift, then from dividing equations 8 by 7 for the case of $C_\theta \to \infty$ we can see by inspection that efficiency is proportional to the ratio of *mean cube* to *mean square* of the

flapping velocity. Thus for efficiency we would expect flapping kinematics to be biased towards triangular flapping profiles.

### 3.2 Selection of the pitching amplitude and the flapping amplitude

The selection of the pitching angle amplitude, $\theta_{\max}$, depends on which design criteria should be prioritised. By inspection, for maximum lift to be generated $\theta_{\max}$ should take a value which maximises the wing *lift coefficient*, which for the present aerodynamic model (see Eqn. 4) occurs with an angle of attack of 45 degrees throughout the flapping half-stroke. The selection of $\theta_{\max} = 45^{\circ}$ is consistent with the usual practise adopted within the analysis process in previous studies (e.g. [4]). On the other hand, if power for a given lift is to be minimised then Eqn. 15, for example, shows that to achieve this design criteria the power factor, *PF*, has to be maximised which in turn is achieved by decreasing the mid half-stroke angle of attack (see also Appendix A).

With regard to selection of the flapping angle amplitude, $\phi_{\max}$, this should always be as large as possible: in terms of effectiveness, larger stroke amplitudes allow higher instantaneous velocity values for the same wing geometry and operational frequency (see Eqn. 2) and hence generation of higher aerodynamic forces; in terms of lift production efficiency, a larger stroke means a larger disk area and hence a lower disk loading. This leads to lower average downwash velocity and reduced induced power expenditure. Furthermore, higher velocity and larger disk area combined leads to lower inflow ratios and thus lower induced losses due to the wake periodicity effect [8].

## 4. Results

### 4.1 Effectiveness and efficiency maps

Further to the qualitative interpretation of the kinematic-aerodynamic model in section 3, we now consider a numerical evaluation in the form of contour maps of effectiveness and efficiency as a function of the flapping and pitching control parameters $C_{\phi}$ and $C_{\theta}$, Fig. 3

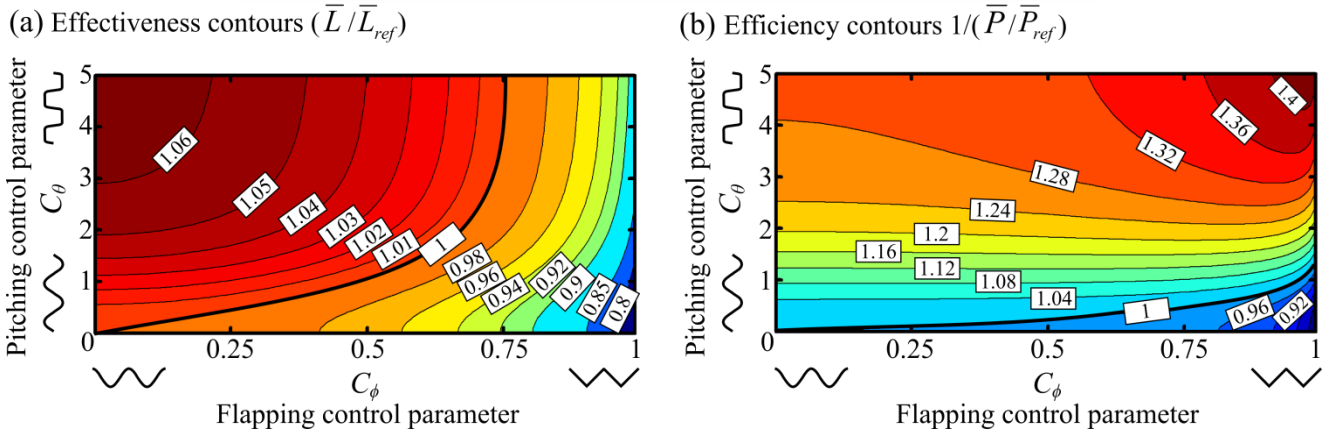


**Figure 3:** Variation of (a) normalised lift, and (b) inverse of the normalised power for a given lift for different combinations of $C_\phi$ and $C_\theta$. The values are normalised with respect to the values obtained for sinusoidal flapping and pitching angle variations. Red indicates 'better' in each case. This demonstration is based on numerical integration of Eqs 7 and 8 with $\theta_{\max}$ value of 45 degrees.

Note that lift and power values are normalised with respect to the lift and power values for sinusoidal flapping and pitching angles variations (i.e. $C_\phi = C_\theta = 0$). Sinusoidal variations of the flapping and pitching angles are used as the reference kinematics because they are simple to implement and also minimise peak acceleration in the wing motion which reduces instantaneous actuator power requirement [23]. Also, the upper bound for the $C_\theta$ parameter was set to 5 representing a practical upper bound for this variable. A value of 5 for $C_\theta$ is equivalent to completing of wing rotation within around 25% of the flapping cycle period, see Fig. 2.

#### *4.1.1 Maximum effectiveness*

Here we wish to identify the wing kinematics that leads to generation of the largest aerodynamic lift force for a given wing geometry and flapping frequency, irrespective of the required power. It is a given that the wing operates at a maximum stroke amplitude. It is found that the kinematics for highest effectiveness are: a sinusoidal variation of the flapping angle (implying sinusoidal variation of the velocity) with a step-like pitching variation of a $\theta_{\max}$ of 45 degrees. This result is consistent with the discussion in section 3 (model interpretation). Lift generated for constant wing geometry and constant translational force

coefficient for different combinations for $C_\phi$ and $C_\theta$ is shown in Fig. 3a where the sinusoidal flapping and step-like pitching variations combination produces 6.5% more lift compared to the sinusoidal reference kinematics.

#### *4.1.2 Maximum efficiency*

Here, minimum power for a given lift constraint is used as the criteria for the kinematic pattern selection. Lift is kept constant for different kinematic motions by adjusting the flapping frequency value. The efficiency contours shown in Fig. 3b are represented as the inverse of the power expended for a given lift for different value combinations of $C_\phi$ and $C_\theta$. It can be seen that the best combination for highest efficiency (lowest power for given lift) is to have a triangular variation of the flapping angle with a step-like pitching angle variation, i.e. a constant flapping velocity and a fixed pitch angle in each half-stroke. These profiles are consistent with those discussed in section 3.1 and are consistent with the higher order calculus of variation computational model result obtained by Taha et al. [18]. They are also similar to the kinematics used by Schenato et al. [24]. On the other hand, the combination of a triangular variation of the flapping angle and a sinusoidal variation of the pitching angle is the least good with respect to aerodynamic efficiency.

For both best effectiveness and best efficiency the optimum pitching angle variation is the step-like (rectangular) variation. Therefore it remains to choose a sinusoidal flapping angle variation for maximum effectiveness or a triangular flapping angle variation for maximum efficiency.

It is noteworthy to mention that the contour values in Fig. 3b are based on numerical integration evaluations with a $\theta_{\max}$ value of 45 degrees. Changing the value of $\theta_{\max}$ will only change the efficiency contour values, but does not change the conclusion that a triangular variation of the flapping angle with a step-like pitching angle variation are the most efficient motion profiles. To further demonstrate this point, Fig. 4 compares the mean aerodynamic power for a given lift values of the ideal motion profiles ($C_\phi = 1$ and $C_\theta \to \infty$) with respect to the reference sinusoidal profiles. This evaluation is based on the quotient

of Eqs 14 and 17. The superiority of the efficiency-optimum combination can be directly seen from the figure and this superiority even improves as the angle of attack decreases which is consistent with the discussion of section 3.2. However within the typical angle of attack operation range for insect-like wings ($25^\circ \le \alpha \le 45^\circ$ [19]), the variation of the curve shown in Fig. 4 is less significant. Note that Fig. 4 represents the highest bound of the efficiency levels that can be achieved.

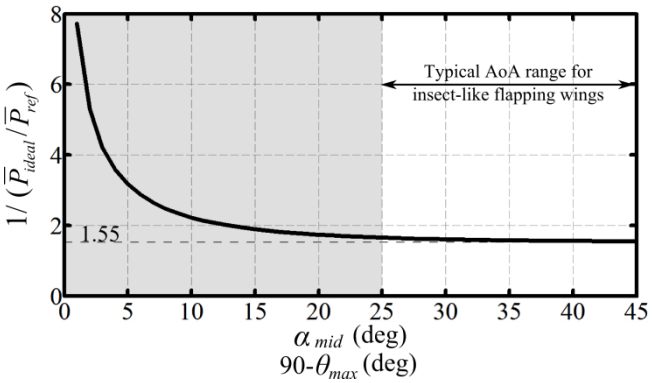


**Figure 4:** Variation of the inverse normalised power for a given lift for the efficiency optimum (ideal) combination ($C_\phi = 1$ and $C_\theta \to \infty$) with geometric angle of attack value. This demonstration is based on the quotient of the analytical expressions of Eqs 14 and 17.

### *4.1.3 Practical implementation of the optimum kinematic profiles*

Whilst the triangular variation of the flapping angle is mathematically elegant, it is challenging from a practical point of view due to the requirement for high acceleration at the end of each half-stroke. Additionally, insect-scale flapping wing vehicles are typically driven at resonance to achieve the large flapping amplitude motion; for a linear transmission system operating at resonance, the output will be sinusoidal by default regardless of the driving waveform [23].

Similarly, rectangular variation of the pitch angle to give rapid reversal of geometric angle of attack at the end of each half-stroke is mechanically more expensive than a sinusoidal variation due to the higher actuation torque required and the fact that resonance cannot be used to amplify this motion. A number of practical flapping wing implementations have successfully used passively generated pitching kinematics in which wing hinge properties are exploited to generate a pitching motion of the correct phase to the

flapping motion [25,5]. Use of a suitably nonlinear structural response, e.g. via implementation of a softening torsional stiffness, can allow passively generated pitching kinematics to more closely approximate the rectangular variation required for both maximum efficiency and maximum effectiveness.

Whilst the combination of a triangular variation of the flapping angle and a rectangular variation of the pitching angle is practically challenging for a flapping wing, it is trivial to implement using a rotary wing. Comparison of Eqs 16 and 17, shows us that sinusoidal flapping velocity expends 20% more aerodynamic power than constant rotary velocity for the same lift. Thus apart from practicality issues, a flapping wing becomes most efficient when it approaches the rotary wing motion. This also support the argument presented in references [26] and [27] that a rotating (spinning or revolving) wing motion is more efficient at generating lift than a flapping motion.

Using the second expression of Eqn. 11, it can be shown that sinusoidal flapping generate 23% more lift compared to triangular flapping for all other variables being the same. Given that a sinusoidal variation in velocity is the most effective solution for a flapping wing at a given frequency, why is it that we do not see this in engineered continuously rotating wings? The answer appears to be that for these systems it is easier mechanically to increase the speed by increasing the frequency than it is to introduce angular velocity variations within each cycle.

Implementation of a sinusoidal flapping angle variation ($C_\phi = 0$) together with a near constant angle of attack within the half-stroke (e.g. using $C_\theta = 5$) represents an appropriate practical solution for two reasons. First, the current relative immaturity of relevant micro-electromechanical system design and manufacturing means the current focus is on achieving the basic requirement of lift greater than or equal to weight. This situation is very similar to the status in the early years of powered flight. As such, any means to achieve higher lift values needs to be exploited. Thus; whilst the lift force generation from sinusoidal flapping with a near constant $45^\circ$ angle of attack kinematics is just 6.5% more than the dual sinusoidal kinematics case, this extra lift may be the marginal lift that allows successful take off. Second, whilst these kinematics ($C_\phi = 0$, $C_\theta = 5$) are 20% below the optimum kinematics with respect to

efficiency, they still provide a 29% higher efficiency level compared to the dual sinusoidal case (see Fig. 3b). This will have a significant effect on the achievable flight duration of the vehicle.

### 4.2 Selection of the flapping frequency, *f*

The flapping frequency, $f$, can always be selected in order to satisfy a given weight constraint; that is, more lift can always be generated by flapping faster. For the present analysis we assume that the angle of attack during each half-stroke is constant (which is consistent with requirements for both efficiency and effectiveness). Thus we calculate flapping frequency from the second formula in Eqn. 13, with $C_\theta \to \infty$. A comparison between predicted and reported flapping frequency for eight hovering insects is given in Table 1. Insect weight, morphological and kinematic data is from Sun and Du [19]. Calculated flapping frequency is obtained from Eqn. 13 using a $C_\phi = 0.001$ and a representative value of 1.1 for the lift coefficient, $C_L$. The obtained results are in close agreement with the frequency values reported by Sun and Du [19] with a mean absolute error of 7.9% and mean error of 0.6% for the eight calculations. Note that accuracy in the predicted frequency can be significantly improved by using lift coefficient values specific to each wing geometry; however, the point we wish to make with the data is that even assuming a universal value of 1.1, the predicted results are still usefully accurate over a broad range of insect sizes and wing geometries.

**Table 1:** Comparison between reported and calculated frequency for eight hovering insects. Weight, morphological and kinematic parameters are based on collected data in [19]. Insects listed in order of increasing mass.

| Insect | mass (mg) | $R$ (mm) | $\bar{c}$ (mm) | $\hat{r}_2$ | $\phi_{\max}$ (deg.) | $f_{reported}$ (Hz) | $f_{calculated}$ (Hz) | error (%) |
|---|---|---|---|---|---|---|---|---|
| **Fruit fly** | 0.72 | 2.02 | 0.67 | 0.596 | 75 | 254 | 281 | +9.6 |
| **Cranefly** | 11.4 | 12.7 | 2.38 | 0.614 | 61.5 | 45.5 | 44.6 | -2.11 |
| **Hoverfly** | 27.3 | 9.3 | 2.2 | 0.578 | 45 | 160 | 166 | +3.7 |
| **Ladybird** | 34.4 | 11.2 | 3.23 | 0.538 | 88.5 | 54 | 63.6 | +15 |
| **Dronefly** | 68.4 | 11.4 | 3.19 | 0.543 | 54.5 | 157 | 141 | -11 |
| **Honey bee** | 101.9 | 9.8 | 3.08 | 0.566 | 65.5 | 197 | 176 | -11.9 |
| **Bumble bee** | 175 | 13.2 | 4.02 | 0.554 | 58 | 155 | 149 | -4 |
| **Hawkmoth** | 1648 | 51.9 | 18.26 | 0.525 | 60.5 | 26.3 | 27.8 | +5.5 |
| | | | | | | Mean absolute error | | 7.88% |
| | | | | | | Mean error | | 0.6% |

## 5. Conclusions

A simple approach for optimum kinematic motion selection of hovering flapping wings has been proposed. Explicit analytical expressions for the average lift and power of the most relevant kinematic motions for hovering flapping flight are derived. These expressions should prove useful for the purposes of preliminary engineering design of flapping wing vehicles and prediction of flapping frequency of insects from weight and morphological data. Flapping and pitching angle variations are identified for achieving maximum effectiveness, and for achieving maximum efficiency.

For effectiveness, the flapping angle profile should be sinusoidal, whereas for efficiency, the flapping angle profile should be triangular, with the pitching angle being rectangular in each case. Operation with maximum effectiveness profiles generates 23% more lift compared to optimum efficiency profiles, and expends 20% more aerodynamic power to produce the same lift compared to optimum efficiency profiles.

A 45 degrees rectangular pitching profile and a sinusoidal flapping profile are the maximum effectiveness profiles producing 6.5% more lift compared to the dual sinusoidal reference case. Whereas, the use of triangular flapping and rectangular pitching profiles increases the maximum attainable efficiency by 55% compared to the dual sinusoidal reference case with a 45 degrees mid half-stroke angle of attack, and this efficiency even improves as the mid half-stroke angle of attack is decreased.

## Appendix A: Evaluation of the effect of skin friction drag on the aerodynamic performance of flapping wings at insect scales

Experimental measurements for insect-like model wings at Reynolds number of $O(10^3)$ or higher have shown that at zero angle of attack the drag coefficient can be sensibly neglected [16,26,27]. However at lower Reynolds number of $O(10^2)$, experiments on fruit fly model wings showed that $C_{D0}$ may be more significant as the Reynolds number decreases [1,26]. To evaluate the effect of the friction tangential force within the lift and drag coefficient relations, Eqns 4 and 5 are modified following [28] as:

$$C_L(\alpha) = C_T \sin(2\alpha) - C_{D0} \cos^2(2\alpha) \sin(\alpha), \quad \text{(A1)}$$

$$C_D(\alpha) = 2C_T \sin^2(\alpha) + C_{D0} \cos^2(2\alpha) \cos(\alpha). \quad \text{(A2)}$$

Fig. A1 shows the variation of the power factor against angle of attack for a range of $C_{D0}$ values, and a fixed $C_T$ value of 1.5. The main outcomes from Fig. A1 are: (1) the power factor increases as the angle of attack decreases within the insect-like flapping operation range; thus to achieve higher efficiency the operational angle of attack should be biased towards low values. (2) As the angle of attack increases, the influence of $C_{D0}$ becomes less significant. Thus for the fruit fly, which operates at a typical mid half-stroke angle of attack of $44^\circ$ [19], the effect of having a high $C_{D0}$ does not significantly affect the flight performance. On the other hand, insects such as the honey bee and bumble bee employ mid half-stroke angle of attack values around $25^\circ$ [19]. However, they operate at Reynolds number of $O(10^3)$ and above where the skin friction drag can be neglected [1,16,26].

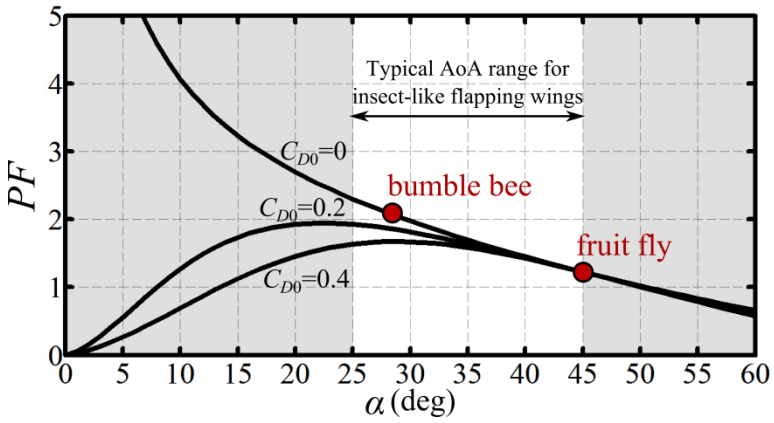


**Figure A1**: Variation of the power factor against angle of attack for a range of skin friction drag values. The highlighted part represents the operating mid half-stroke angle of attack range for most insects between 25 to 45 degrees.

**References:**


1. Berman, G. J., Wang, Z. J. 2007 Energy-minimizing kinematics in hovering insect flight. *J. Fluid Mech*., **582**, 153–168. (doi 10.1017/S0022112007006209)
2. Wang, Z. J. 2008 Aerodynamic efficiency of flapping flight: analysis of a two-stroke model. *J. Exp. Biol.*, **211**, 234-238. (doi 10.1242/jeb.013797)
3. Pesaveno, U., Wang, Z. J. 2009 Flapping wing flight can save aerodynamic power compared to steady flight. *Physical Review Letters*, **103**, 118102. (doi 10.1103/PhysRevLett.103.118102)
4. Ansari, S. A., Knowles, K., Zbikowski, R. 2008 Insectlike flapping wings in the hover part 1: effect of wing kinematics. *J. Aircraft*, **45**, 1945-1954. (doi 10.2514/1.35311)
5. Khan, Z. A., Agrawal, S. K. 2011 Optimal hovering kinematics of flapping wings for micro air vehicles. *AIAA J.* **49**, 257-268. (doi 10.2514/1.J050057)
6. Liu, Y., Sun, M. 2008 Wing kinematics measurement and aerodynamics of hovering droneflies. *J. Exp. Biol.* **211**, 2014–2025. (doi 10.1242/jeb.016931)
7. Wang, Z. J. 2005 Dissecting insect flight. *Annu. Rev. J. Fluid Mech*. **37**, 183–210. (doi 10.1146/annurev.fluid.36.050802.121940)
8. Nabawy, M. R. A., Crowther, W. J. 2014 On the quasi-steady aerodynamics of normal hovering flight part I: the induced power factor. *J. R. Soc. Interface* **11**: 20131196. (doi 10.1098/rsif.2013.1196)
9. Nabawy, M. R. A., Crowther, W. J. Is flapping flight aerodynamically efficient? 32nd AIAA Applied Aerodynamics Conference, AIAA Aviation and Aeronautics Forum and Exposition, 16 - 20 June 2014, Atlanta, Georgia, USA. (doi: 10.2514/6.2014-2277)
10. Altshuler, D. L., Dickson, W. B., Vance, J. T., Roberts, S. P., Dickinson, M. H. 2005 Short-amplitude high-frequency wing strokes determine the aerodynamics of honeybee flight. *Proc. Natl. Acad. Sci. U.S.A.* **102**, 18213-18218.

11. Liu, Y., Sun, M. 2007 Wing kinematics measurement and aerodynamic force and moments computation of hovering hoverfly. Proceedings of the 1st International Conference on Bioinformatics and Biomedical Engineering, Wuhan, China, 6-8 July 2007, 452-455. (doi: 10.1109/ICBBE.2007.119)
12. Elzinga, M. J., van Breugel, F., Dickinson, M. H. 2014 Strategies for the stabilization of longitudinal forward flapping flight revealed using a dynamically-scaled robotic fly. *Bioinspir. Biomim*, **9**, 025001. (doi:10.1088/1748-3182/9/2/025001)
13. Willmott, A. P., Ellington, C. P. 1997 The mechanics of flight in the hawkmoth Manduca sexta. I. Kinematics of hovering and forward flight. *J. Exp. Biol.*, **200**, 2705-2722.
14. Wu, J. H., Sun, M. 2012 Floquet stability analysis of the longitudinal dynamics of two hovering model insects. *J. R. Soc. Interface* **9**, 2033-2046. (doi:10.1098/rsif.2012.0072)
15. Nabawy, M. R. A., Crowther, W. J. 2014 On the quasi-steady aerodynamics of normal hovering flight part II: model implementation and evaluation. *J. R. Soc. Interface* **11**: 20131197. (doi 10.1098/rsif.2013.1197)
16. Usherwood, J. R., Ellington, C. P. 2002 The aerodynamics of revolving wings: I. Model hawkmoth wings. *J. Exp. Biol.* **205**, 1547–1564.
17. Lau, G. K., Chin, Y. W., Goh, J. W., Wood, R. J. 2014 Dipteran-insect-inspired thoracic mechanism with nonlinear stiffness to save inertial power of flapping-wing flight. *IEEE Transactions on Robotics*. (doi 10.1109/TRO.2014.2333112)
18. Taha, H. E., Hajj, M. R., Nayfeh, A. H. 2013 Wing kinematics optimization for hovering micro air vehicles using calculus of variation. *J. Aircraft*, **50**, 610-614. (doi 10.2514/1.C031969)
19. Sun, M., Du, G. 2003 Lift and power requirements of hovering insect flight, *Acta Mechanica Sinica* **19**, 458–469. (doi 10.1007/BF02484580)
20. Ellington C. P. 1984 The aerodynamics of hovering insect flight: VI. Lift and power requirements. *Phil. Trans. R. Soc. Lond. B* **305**, 145-181. (doi 10.1098/rstb.1984.0054)
21. Whitney, J. P., Wood, R. J. 2012 Conceptual design of flapping-wing micro air vehicles. *Bioinspir. Biomim.* **7**, 036001. (doi 10.1017/S002211201000265X)
22. Kruyt, J. W., Quicazan-Rubio, E. M., van Heijst, G. J. F., Altshuler, D. L., Lentink, D. 2014 Hummingbird wing efficacy depends on aspect ratio and compares with helicopter rotors. *J. R. Soc. Interface* **11**: 20140585. (doi 10.1098/rsif.2014.0585)
23. Nabawy, M. R. A., Parslew, B. Crowther, W. J. 2014 Dynamic performance of unimorph piezoelectric bending actuators. *Proc. Inst. Mech. Eng. I J. Syst. Control Eng.* **229**, 118-129. (doi 10.1177/0959651814552810)
24. Schenato, L., Campolo, D., Sastry, S. 2003 Controllability issues in flapping flight for biomimetic micro air vehicles (MAVs). Proceedings of the 42nd IEEE Conference on Decision and Control, Maui, HI, USA, 9-12 December 2003, vol.6, 6441-6447. (doi: 10.1109/CDC.2003.1272361)
25. Whitney, J. P., Wood, R. J. 2010 Aeromechanics of passive rotation in flapping flight. *J. Fluid Mech*. **660**, 197-220. (doi 10.1088/1748-3182/7/3/036001)
26. Lentink, D., Dickinson, M.H. 2009 Rotational accelerations stabilizes leading edge vortices on revolving fly wings. *J. Exp. Biol.* **212**, 2705–2719.

27. Lentink, D., Jongerius, S. R., Bradshaw, N. L. 2010 The scalable design of flapping micro-air vehicles inspired by insect flight. In *Flying Insects and Robots*, (ed. Floreano, D., Jean-Christophe Zufferey, J-C., Mandyam V. Srinivasan, M. V. & Ellington C.), Ch. 14, Springer, 185–205.
28. Wood, R. J., Whitney, J. P., Finio, B. M. 2010 Mechanics and actuation for flapping-wing robotic insects. In *Encyclopedia of Aerospace Engineering*, (ed. Blockley, R. & Shyy, W), Ch. 357, John Wiley & Sons, Ltd., 4393–4405.